THE BELL SYSTEM TECHNICAL JOURNAL
Vol. 61, No. 9, November 1982
Printed in U.S.A.

A Statistical Model of Multipath Fading on a Space-Diversity Radio Channel

By W. D. RUMMLER

(Manuscript received February 22, 1982)

The joint probability of occurrence of frequency-selective fades on a pair of spatially separated receiving antennas is modeled for a typical line-of-sight microwave radio path in the 6-GHz band. The model was developed from observations of the transmission in a 24.2-MHz band during all multipath-fading occurrences in a 30-day period on a 26.4-mile path. By fitting the observations of every scan on both antennas with a simplified three-ray channel modeling function, the joint transmission at each observation is characterized by six parameters, three for each antenna. The joint occurrence of these six parameters is described by simple statistical distribution functions, allowing one to associate with any pair of channel transmission shapes the fraction of a year, or number of seconds in a year, that such a channel state will be encountered. The model represents the frequency selectivity or shape of the fades on the two antennas as statistically independent. Only the average fade levels on the two antennas are statistically related. Either antenna is more likely to experience a fade deeper than the median when selectivity is observed on it or when the other antenna is experiencing deeper fading than the median. The (marginal) statistics of fading on each of the antennas separately, as derived from the diversity model, are essentially the same as those described by a nondiversity statistical fading model, which has been used successfully to predict the multipath outage of digital radio systems. The model developed here will allow performance to be estimated in a diversity configuration.

I. INTRODUCTION

Occurrences of multipath fading limit the performance quality of high-speed digital radio systems operating on line-of-sight microwave radio paths. Extensive field measurement programs have been imple-

mented to evaluate the performance of a number of digital radio systems operating in different configurations under various conditions.[1-5] These studies have indicated the universal need for some form of dynamic channel equalization, and for space diversity reception, on many paths, to meet performance requirements. While field measurements provide a good means of evaluating the operation of radio systems, they require considerable time, effort, and expense. Furthermore, they suffer from the vagaries of nature in that multipath fading is a randomly occurring phenomenon with variable characteristics from month to month.[5,6]

To reduce the need for field measurements, a statistical model of multipath fading was developed.[6,7] This model, used in conjunction with characterization measurements performed on a radio in the laboratory, allows predictions to be made of the system performance under multipath conditions when operating in a nondiversity configuration.[8-10] The results presented here extend the previous work by providing a statistical model for multipath fading in a space-diversity configuration.

The data base used for modeling was obtained by transmitting a wideband (8-PSK digital radio) signal at 6 GHz over a 26.4-mile path from Atlanta to Palmetto, Georgia. The received power at a number of frequencies in a 24.2-MHz band was measured simultaneously on both a horn reflector and a parabolic dish antenna separated by 30 feet. Spectra were observed at rates up to five times per second during the occurrences of multipath propagation in a 30-day period in August to September, 1977. The received voltages on both the horn and dish at each observation, relative to unfaded or free-space propagation conditions, are represented as a function of frequency by the simplified three-path modeling function that has the form

$$H(j2\pi f) = a[1 - be^{-j2\pi(f-f_0)\tau}]. \tag{1}$$

The diversity channel model provides a joint statistical representation of the occurrence of the parameters of the function (1) as fitted for both the horn and dish.

The choice of a modeling function for representing selective multipath fades over a restricted frequency band is not unique. Such a function needs only to be capable of representing the characteristics of a multipath fade. The parameter statistics will depend strongly on the choice of function. Greenstein and Czekaj[11] have used a complex polynomial in frequency to represent multipath fades and have developed statistics for the coefficients of the polynomial for a nondiversity data base. Although other modeling functions have been proposed,[12-17] none has been successfully represented on a statistical basis. The modeling function (1) used here has the virtues of providing an

excellent representation of the observed multipath fades and of being convenient for synthesis in the laboratory for the stressing of radio systems for performance appraisal. In the present work we show that a further advantage of this function is that the joint statistics in a diversity configuration are well behaved and easily represented.

The statistical channel model is summarized in Section II. The data base used and the fitting of observations with the modeling function are described in Section III. In Section IV we provide the methodology for developing and verifying the statistical model. Concluding remarks are provided in Section V.

II. MODEL SUMMARY

2.1 Modeling function

During multipath fading, the voltage transfer functions of the paths to the horn reflector and to the parabolic dish antenna are modeled by

$$H_H(j2\pi f) = a_H[1 - b_H e^{-j2\pi(f-f_{0H})\tau}] \tag{2}$$

and

$$H_D(j2\pi f) = a_D[1 - b_D e^{-j2\pi(f-f_{0D})\tau}], \tag{3}$$

respectively. These transfer functions are measured relative to the unfaded, or free-space, transfer functions, which are both taken as unity at all frequencies, f. For convenience and for consistency with previous work we fix the delay τ at 6.3 ns. These functions may be interpreted as the responses of channels with direct transmission paths with amplitudes a_H and a_D, and second paths with relative amplitudes b_H and b_D, both respectively. The second path in each case has a relative delay of 6.3 ns, and a phase of $2\pi f_{0H}\tau + \pi$ and $2\pi f_{0D} + \pi$ (independently controllable) at the center frequency of the channel.

A typical plot of the attenuation produced by such modeling functions is shown in Fig. 1. The a and b parameters control the depth and shape of the simulated fades, respectively. The parameters f_{0H} and f_{0D} determine the frequencies of the transmission minima, or notches, of the simulated fades. With a simulated minimum within the channel, the modeling functions can simulate a wide range of levels and notch widths. With a simulated minimum out of the channel band, the modeling functions can generate a wide range of combinations of levels, slopes, and curvatures of the in-band responses.

For convenience we work with the following related parameters: the fade-level parameters (in decibels)

$$A_H = -20 \log a_H \tag{4}$$

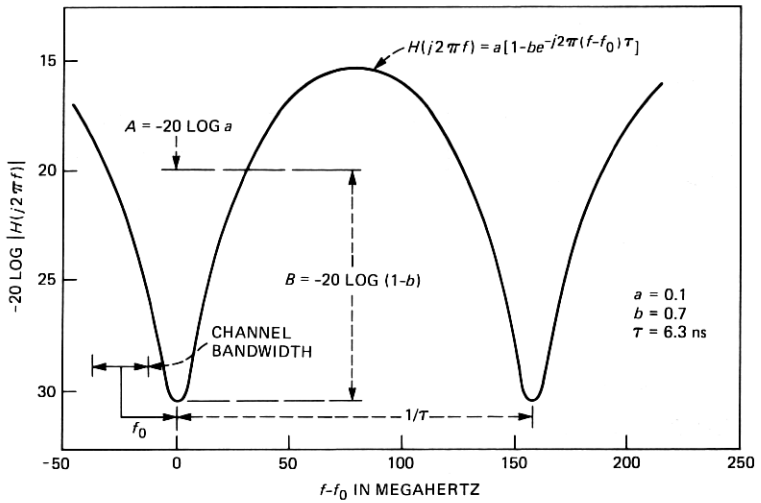

Fig. 1—Attenuation of channel modeling function.

and

$$A_D = -20 \log a_D; \tag{5}$$

the relative notch depth parameters (in decibels),

$$B_H = -20 \log(1 - b_H) \tag{6}$$

and

$$B_D = -20 \log(1 - b_D); \tag{7}$$

and the notch frequency parameters, which we measure in degrees,

$$\phi_H = 360 f_{0H} \tau \tag{8}$$

and

$$\phi_D = 360 f_{0D} \tau. \tag{9}$$

With τ equal to 6.3 ns, one degree in ϕ corresponds to 0.44 MHz. We measure notch frequencies, ϕ, from the center frequency of the channel, so that ϕ covers the range from −180 to +180 degrees, corresponding to the 158.4-MHz period of the functions (2) and (3).

2.2 Parameter statistics

The number of seconds in a year that the six parameters (A_H, A_D, B_H, B_D, ϕ_H, ϕ_D) are in a differential element of the six-dimensional parameter space is shown to be given by

$$T(A_H, A_D, B_H, B_D, \phi_H, \phi_D)$$
$$= T_0 p_{A/B}(A_H, A_D/B_H, B_D) p_{B_H}(B_H) p_{B_D}(B_D) p_H(\phi_H) p_D(\phi_D), \quad (10)$$

where the functions $p(\cdot)$ are all probability density functions. The time scale factor T_0, under the assumption that events scale with the classical scaling of the incidence of multipath fading,[18] is given by the expression:

$$T_0 = 52800c(f/6)(D/25)^3 \quad (11)$$

where

f is the frequency in GHz,
D is the path length in miles, and
c is the terrain factor, varying between 0.25 and 4.

The probability density functions of horn and dish relative notch depths are given, respectively, by

$$p_{B_H}(B_H) = 0.76711(2B_H)(0.10258)e^{-0.10258B_H^2} + 0.23289(0.23281)e^{-0.23281B_H} \quad (12)$$

$$p_{B_D}(B_D) = 0.82295(2B_D)(0.07668)e^{-0.07668B_D^2} + 0.17705(0.21786)e^{-0.21786B_D}. \quad (13)$$

The joint probability density function of A_H and A_D is conditioned on the values of B_H and B_D and is given by

$$p_{A/B}(A_H, A_D | B_H, B_D) = \frac{1}{2\pi\sigma_H\sigma_D\sqrt{1-\rho^2}} \exp\frac{-1}{2(1-\rho^2)}\left[\frac{(A_H - g_H)^2}{\sigma_H^2} - \frac{2\rho(A_H - g_H)(A_D - g_D)}{\sigma_H\sigma_D} + \frac{(A_D - g_D)^2}{\sigma_D^2}\right], \quad (14)$$

where

$$g_H = g_H(B_H) = 23.956(701.11 + B_H^4)/(1320.6 + B_H^4) \quad (15)$$

$$g_D = g_D(B_D) = 27.139(1223.8 + B_D^4)/(2650.9 + B_D^4) \quad (16)$$

and

$$\sigma_H = 6.8268$$
$$\sigma_D = 7.0272$$
$$\rho = 0.64995. \quad (17)$$

The probability density functions for the horn and dish notch frequencies are given, respectively, by

$$p_H(\phi_H) = \begin{cases} \dfrac{5}{1080} & |\phi_H| < 90 \\ \dfrac{1}{1080} & 90 \le |\phi_H| < 180 \end{cases} \tag{18}$$

and

$$p_D(\phi_D) = \begin{cases} \dfrac{8}{1620} & |\phi_D| < 90 \\ \dfrac{1}{1620} & 90 \le |\phi_D| < 180. \end{cases} \tag{19}$$

2.3 Interpretive discussion

The salient features of the model, which are verified in Section 4, are easily stated. The selective components of multipath fading as seen by the horn and the dish are modeled as independent processes. This means that detailed knowledge of the transmission "shape" present at a given instant on one antenna provides no information concerning the shape that will be present on the other. The only coupling between the fading on the two antennas is provided through the joint conditional A-distribution of (14). The form of this conditional probability density function implies that the fade-level parameters, or fading levels, on the two antennas are related. Deeper fades on one tend to be accompanied by deeper fades on the other. The conditioning on the relative notch depth parameters implies that the fade-level parameters depend on the fade shapes. This is similar to the coupling provided in the nondiversity model[6,7] in that the fade-level parameter is correlated with relative notch depth, or that deeper fades are more likely to occur when shape is present. For the diversity model we find that the existence of a shapely fade on one antenna is more likely to be accompanied by deeper than average fading on the other.

There are two important limitations of the proposed model. The most obvious limitation is that we have not explicitly represented the variability in fading statistics that would accompany changes in relative spacing in the two receiving antennas. At first blush, we ascribe this to the existence of only one data base for the particular configuration tested; hence, the model is only valid for antenna spacings of thirty feet. Upon closer inspection, one notes that the only coupling parameter that is unique to the diversity configuration is the parameter ρ in the joint conditional A-parameter distribution. (With $\rho = 0$, the model would factor into two independently fading probability models.) One could, in principle, relate ρ to antenna separation by calculating the single-frequency fade statistics of a simulated diversity switch as a function of ρ and compare these results with the known results for various antenna separations.[19] While an extrapolation of the model to

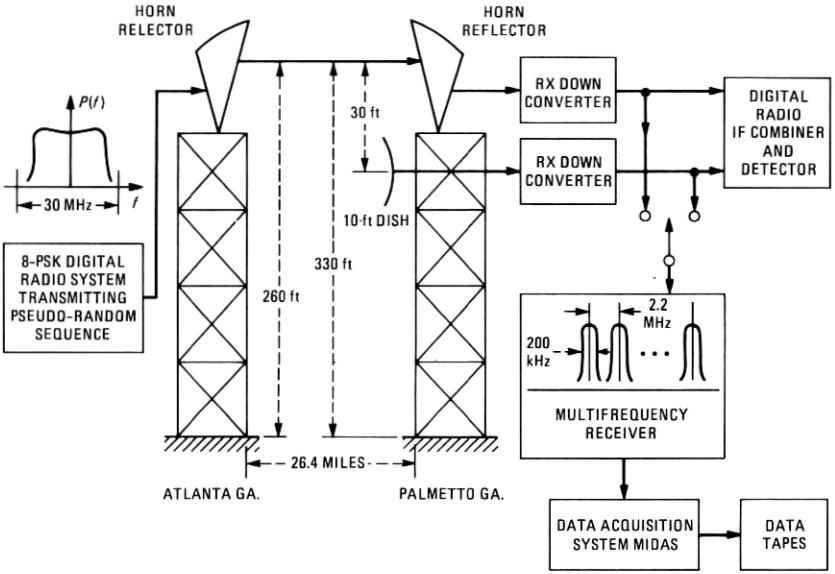

Fig. 2—Experimental configuration for diversity propagation measurements, August 8 to September 6, 1977.

larger separations is straightforward, one would expect that for sufficiently small antenna separations the fade shapes observed on the two antennas would be correlated, leading to a more complicated model.

The other model limitation results from the lack of phase information in the channel probing measurements. We model the channel as a minimum phase channel at all times; that is,[20] we choose a solution with $0 \leq b \leq 1$ and assume a minus sign for the $f\tau$ term in the exponential in (2) and (3). This limitation makes it difficult to assess the characteristics of the combined signal for a continuously adaptive space-diversity combining algorithm.

III. PROPAGATION MEASUREMENTS AND THEIR REPRESENTATION

3.1 Description of the propagation experiment

The propagation measurements used in this study were obtained from an experiment conducted on a 26.4-mile path from Atlanta to Palmetto, Georgia, during the period from August 8 to September 6, 1977. Many of the parameters of the experiment are summarized in Fig. 2. The radiated signal source was a general trade 78-Mb/s, 8-PSK digital radio operating at a nominal center frequency of 6034.2 MHz. The signal was received at Palmetto on both a standard horn reflector and a 10-foot diameter parabolic dish located 30 feet below the horn. The spectral energy received by each antenna was measured at 12

frequencies separated by 2.2 MHz and spanning 24.2 MHz. The receiving filter at each of these frequencies had a 200-kHz bandwidth.

During fading activity the received power at each frequency on both antennas was measured either five times a second or once every two seconds, depending on how rapidly the channel was changing. Sampled power, quantized in 1-dB steps, was recorded by the Multiple Input Data Acquisition System (MIDAS), constructed by G. A. Zimmerman. During nonfading periods the power was recorded at a rate of once every thirty seconds. Based on a two-hour measurement period spanning noon on each day, free-space, or nonfaded, received power levels were determined for each frequency.

3.2 Diversity data base

Over the duration of this experiment, multipath fading occurred in fourteen separate time periods. The measurements made in each of these time periods were calibrated and collected into a computer data base for further analysis. The overall data base includes 85,410 scans of both the horn and the dish, and encompasses 44,386 seconds of fading activity.

Although propagation was monitored for approximately one month in the heavy fading season for this path, the observed fading activity was about twice the amount that would be expected in a typical heavy fading month. Figure 3 shows the time-faded statistics for the horn; it shows the number of seconds that power was faded to or below the level specified by the abscissa. (For purposes of analysis, it is assumed that measured or calculated parameters hold a constant value from one observation time instant until the next observation time instant at which the value may make a stepwise change.) The four curves shown represent the power measured at a frequency near the upper end of the frequency band, one near mid-band, and a third near the lower edge of the band. The fourth curve represents the fading of the average power, based upon a wideband measurement of the received signal. We observe that the four curves are virtually coincident down to the 40-dB level, where the rms power characteristically rolls off more rapidly. The coincidence of the curves indicates a good mix of fading events with no dominant events causing an excess of fading activity at any particular frequency in the band.

Also shown in Fig. 3 is the fading activity predicted for this hop in a heavy fading month.[18] The observed fading statistics match the predicted L^2 slope of the predicted curve; however, for this period we have obtained twice as much time at a given level as one would expect in a heavy fading month.

Figure 4 shows the time-faded statistics as observed on the dish antenna. The general observations made for the horn apply here also,

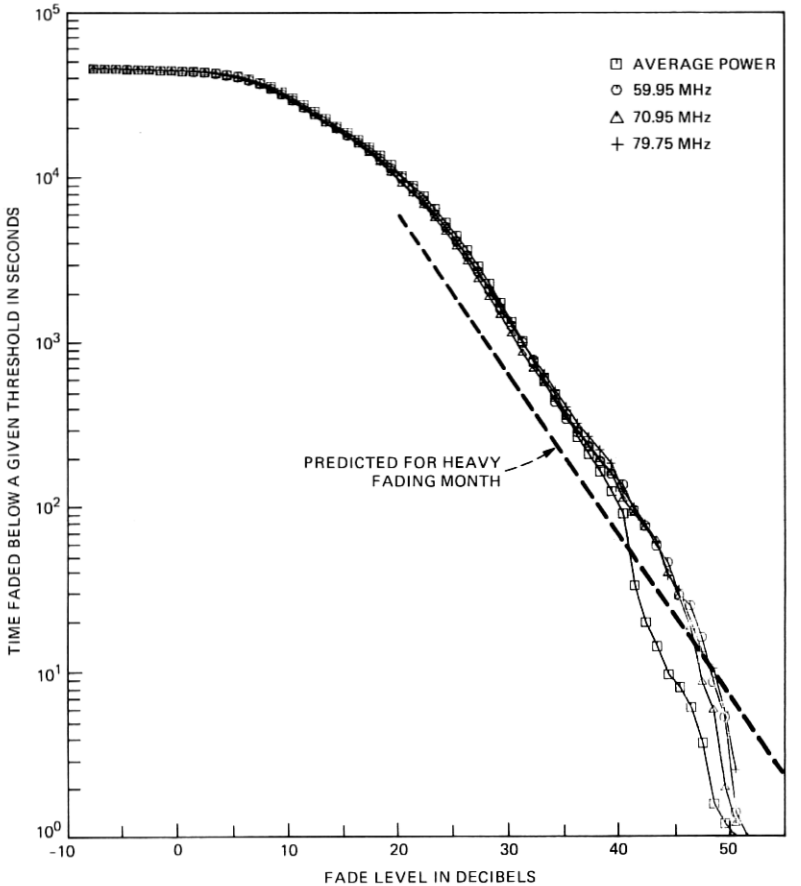

Fig. 3—Time-faded statistics of received power on the horn reflector.

except that we note that the lower frequencies in the band show more fading activity than the upper frequencies at fade levels near 40 dB. The effects of this will become more apparent in Section 4.4. Comparing the dish fading statistics with the predicted fading curve, we would expect the observed fading activity in 2.5 heavy fading months.

As a further consistency check, we consider the in-band power difference (IBPD) statistics, which have also been used for sizing data bases of fading observations.[10] When fading is monitored at a number of frequencies in a band, one can characterize the transmission shape of an observed channel by IBPD, which is the difference, in decibels, between the largest and smallest attenuation of the observed frequencies at a given time. Figure 5 shows the IBPD statistics for the horn and the dish; that is, it shows the number of seconds that the IBPD equaled

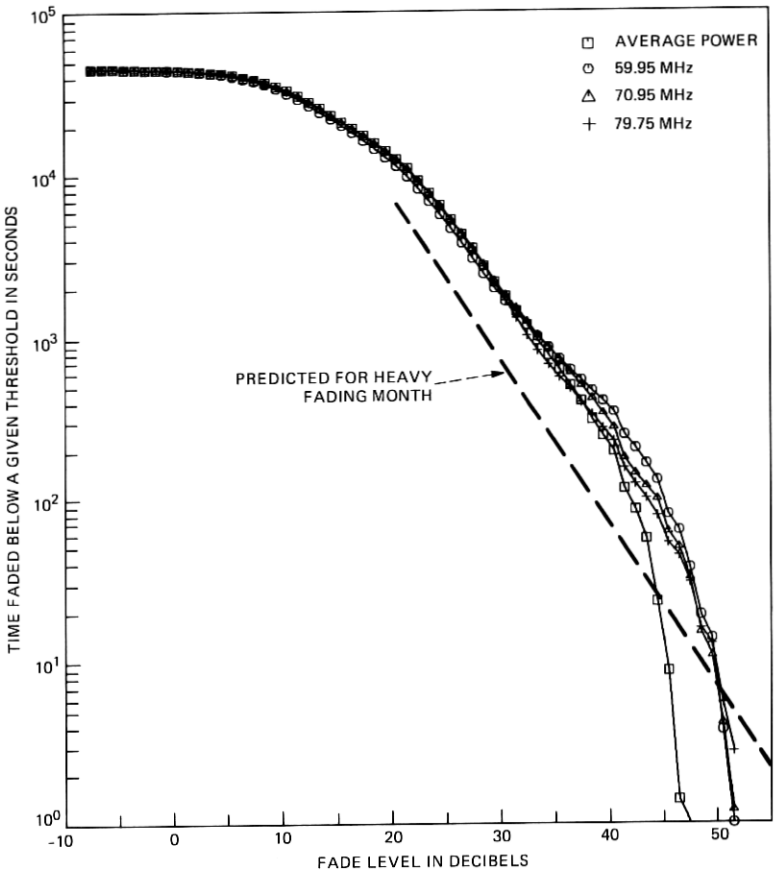

Fig. 4—Time-faded statistics of received power on the dish antenna.

or exceeded the value specified by the abscissa. As a reference curve we also show, in Fig. 5, the IBPD curve (see Ref. 8, Fig. 20) derived from the data base used for the nondiversity model[7] as scaled to a heavy fading month. The reference IBPD curve was derived from 23 observed frequencies spanning a 25.3-MHz band. Although the IBPD ascribed to a given channel condition depends upon the frequency band spanned by the observations and, to a lesser extent, on the number of frequencies observed, the bandwidth difference is small, and the effects of frequency spacing may be minimized by concentrating on the more modest values of IBPD, 5 to 10 dB. Over this range of IBPD there are 1.8 to 2.3 times as many seconds at a given level for the horn, and 2.3 to 2.7 times as many seconds for the dish. The midpoints of these ranges are very nearly equal to the scaling factors determined previously from the time-faded statistics.

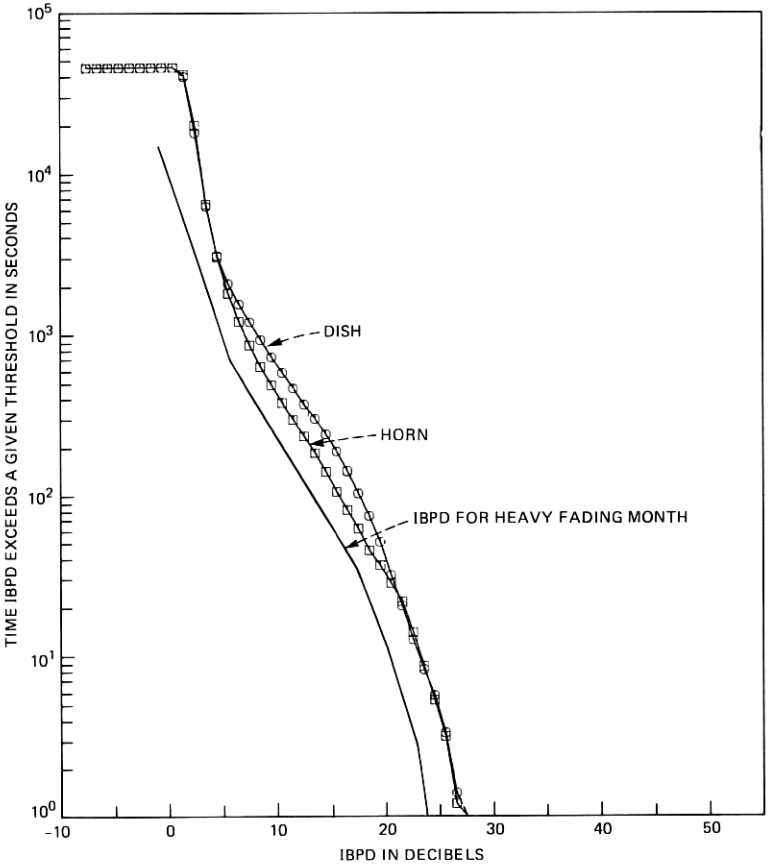

Fig. 5—Time-faded statistics of in-band power difference (IBPD) of the horn and dish.

Splitting the difference between the 2.0 and 2.5 months-of-fading estimates for the horn and dish, respectively, the data base is taken as representing 2.25 months of multipath fading. On the basis that three heavy fading months are equivalent to the fading activity in a year, we take the data base as representing 0.75 of the expected annual multipath-fading activity for this path.

3.3 Representation of spectral measurements

Each scan of the received power levels of the horn and dish is represented by the channel transfer functions (2) and (3), respectively. To obtain the parameters of the functions for each scan, we fit the squared magnitudes of the functions to the received powers. The fitting procedure minimizes the weighted mean squared error between the observed power and the estimated power. The weighting function

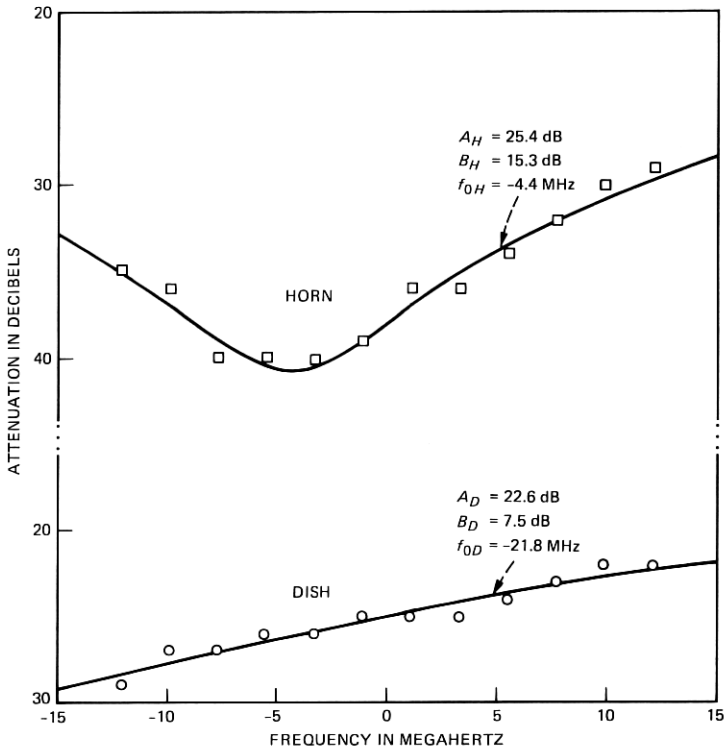

Fig. 6—Representation of fades observed on the horn and dish on August 21, 1977, at 1:28:3.2.

is proportional to the reciprocal of the square of the received power at each frequency. This provides a weighting that is approximately logarithmic, to match the instrumentation errors which are independent and approximately Gaussian on a logarithmic scale. The reader is referred to Ref. 7 for additional details of the fitting procedure.

Figure 6 shows the fits to horn and dish scans observed concurrently. At this particular instant there was a notch present on the horn at a frequency of 4.4 MHz below the band center, and a 6-dB slope present on the dish. The parameter values producing the fitting functions are shown on the plots. The rms error between the observed levels and the values of the fitted function at these frequencies may be taken as a measure of the quality of the representation of the fade. For the horn scan shown, the rms error is 0.68 dB, for the dish 0.50 dB. These values are typical for the measurement system. The power measurement at each frequency has associated with it a fluctuation, or noise, that is additive and approximately Gaussian on a decibel scale. This noise is

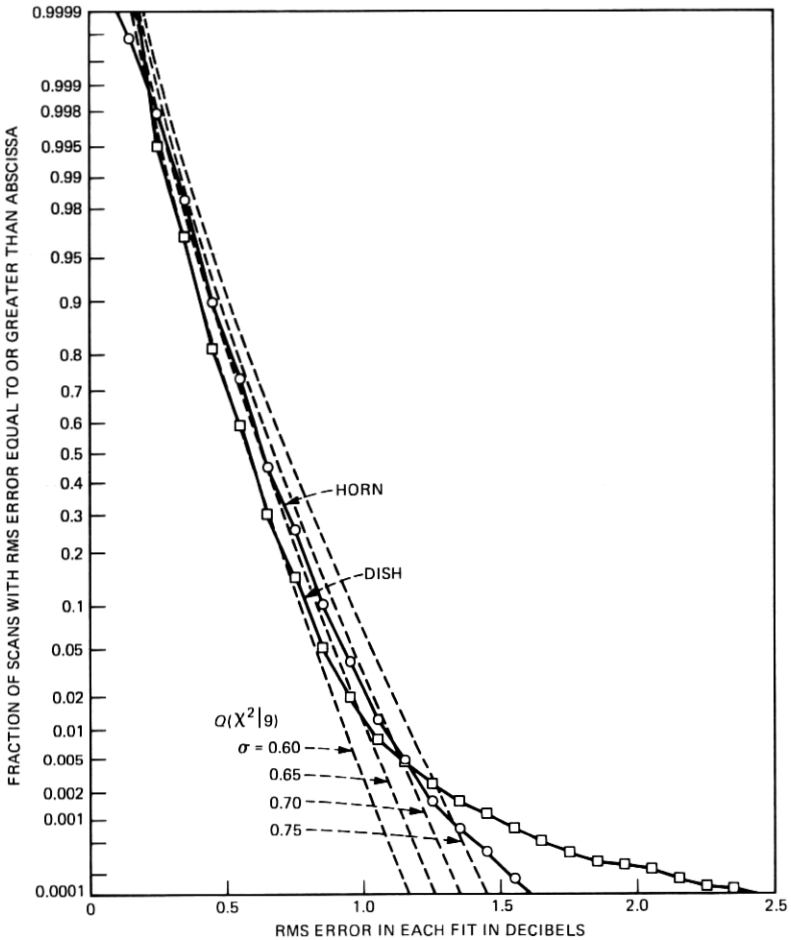

Fig. 7—Distribution of rms fit errors.

independent both frequency-to-frequency and scan-to-scan, and is large enough (0.6 to 0.7 dB) to mask quantization errors.

If the differences between measured and estimated powers were due solely to Gaussian fluctuations with a standard deviation, σ, the quantity $12E_{\text{rms}}^2/\sigma^2$ would be a χ^2 random variable with nine degrees of freedom,[6,7] where E_{rms} is the rms error in fitting a scan. Thus, one can determine the quality of the modeling by comparing the distribution of the values of E_{rms} for all the horn or dish scans with that of a χ^2 variable. The distribution of the horn and dish rms errors are plotted in Fig. 7 along with the χ^2 distributions for several σ values. The excess error, the difference between a sample distribution and a χ^2 distribution

that matches it at the median, is more than 0.1 dB for less than 1 percent of all scans. Because the time between scans is not identical, there is no precise method of scaling the percentages in Fig. 7 to seconds per year. However, an approximate scaling is achieved by applying the percentage to the time covered by the data base and interpreting the resultant time as representing 0.75 of a year. On this basis the excess error in fitting the dish data exceeds 0.5 dB for about 40 seconds a year. For the horn data the excess error is less than 0.4 dB over the entire data base. We conclude that the fitting is exceptionally good for the horn and better than average[6] for the dish.

IV. VERIFICATION OF MODEL STATISTICS

4.1 Overview

We shall begin our discussion with a description of the general modeling problem. By drawing on the properties of probability density functions and on past experience in modeling-selective fading, we will simplify the problem, somewhat. We conclude this subsection with a statement of the objectives of the remainder of the section.

By representing each scan of the horn and the dish with (2) and (3), we obtain a reduced data base consisting of 85,410 sextuples of values of $(A_H, A_D, B_H, B_D, \phi_H, \phi_D)$. Each of these sextuples has associated with it a time weighting corresponding to the time interval until the next scan in the same fading event. We wish to describe this data by a function, $T_D(A_H, A_D, B_H, B_D, \phi_H, \phi_D)$, whose values are equal to the number of seconds the six parameters were in a differential element of the parameter space, centered on the point $(A_H, A_D, B_H, B_D, \phi_H, \phi_D)$. Normalizing T_D to the data base time span, we obtain a probability density function,

$$p(A_H, A_D, B_H, B_D, \phi_H, \phi_D) = T_D(A_H, A_D, B_H, B_D, \phi_H, \phi_D)/44386. \quad (20)$$

It is this probability density function that we wish to determine. We will ultimately show that it may be approximated by the product of the probability functions in (10).

To simplify (20), let us first rewrite it as

$$p(A_H, A_D, B_H, B_D, \phi_H, \phi_D) = p_{AB/\phi}(A_H, A_D, B_H, B_D | \phi_H, \phi_D) p_\phi(\phi_H, \phi_D). \quad (21)$$

In previous work where multipath fading on a single antenna was statistically modeled,[6,7] it was found that the notch frequency statistics were not related to the relative notch depth statistics or to the fade-level statistics. An examination of the current data base revealed the same properties, that is, the statistics of ϕ_H do not depend on those of A_H or B_H, those of ϕ_D do not depend on those of A_D or B_D. Under the

assumption that a cross-coupling (between ϕ_H and A_D, for instance) is even less likely, it was assumed at the outset that (21) can be written as

$$p(A_H, A_D, B_H, B_D, \phi_H, \phi_D) = p_{AB}(A_H, A_D, B_H, B_D)p_{\phi}(\phi_H, \phi_D). \quad (22)$$

We rewrite (22) as

$$p(A_H, A_D, B_H, B_D, \phi_H, \phi_D) = p_{A/B}(A_H, A_D | B_H, B_D)p_B(B_H, B_D)p_{\phi}(\phi_H, \phi_D). \quad (23)$$

In the remainder of this section we shall derive the functional form of each of the probability density functions in (23). The ultimate objective is to show that (23) can be represented by the factors multiplying T_0, on the right-hand side of (10), with the various probability density functions as defined in (12) to (19). To this end, we consider the joint distribution of B_H and B_D in Section 4.3; we show that it can be represented as the distribution of two independent variables with distributions given by (12) and (13). The form of the conditional distribution $p_{A/B}(A_H, A_D | B_H, B_D)$, as given in (14) to (17), is derived in Section 4.3. In Section 4.4, we consider the notch frequency distribution and show that it can be modeled by independent random variables as given by (18) and (19).

As part of the process of developing a multidimensional statistical model one must make many choices that may seem arbitrary. However, we have proceeded with the philosophy that we should represent the data well whenever there is a significant degree of fading present in either antenna. To accurately represent the most severe events, we must develop our cumulative distribution functions from the more severe to the less severe fades, i.e., the complement of the usual cumulative distribution function. Our goal is to find the simplest probability functions that match these distribution functions, where we define simplest functions as those having the fewest possible number of parameters. In assessing how well these objectives are achieved, we view the composite data base as a member of an ensemble of all possible data bases. Thus, the parameters obtained from the data base must be considered as random variables of this ensemble of fading events.

4.2 Notch depth statistics

The objective of the diversity model is to accurately represent the transmission shapes present on both the horn and dish at any time that deep or shapely fading was present on either. In previous work with the nondiversity model it was only necessary to represent the notch depth parameter at values large enough to produce several

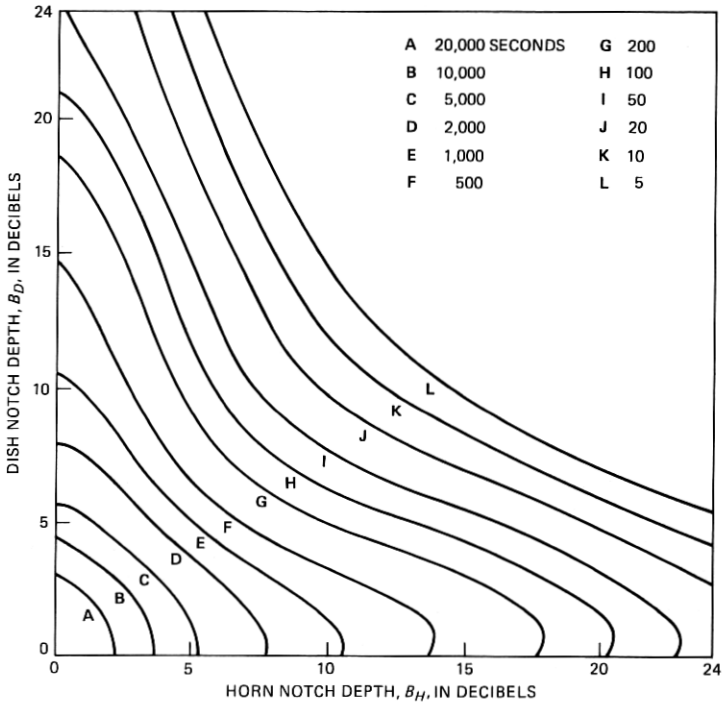

Fig. 8—Contour plot of $\hat{F}(B_H, B_D)$, smoothed fit to cumulative joint distribution function of horn and dish relative notch depths.

decibels of shape in the band. For the diversity model considered here, we must represent the joint distribution of horn and dish notch depth parameters at all values. (While one could give less importance to the distribution in regions where both notch depth parameters are small, this is found to be unnecessary.) We first develop the complement of the cumulative distribution of the sample values of the horn and dish relative notch depths, B_H and B_D, respectively. We define this two-dimensional function, $F(x, y)$, as the number of seconds in the data base that B_H equaled or exceeded a value x, and B_D equaled or exceeded y:

$$F(x, y) = \text{Number of seconds: } B_H \geq x, \ B_D \geq y. \tag{24}$$

To provide a focus for the ensuing discussions, we develop the function $\hat{F}(x, y)$, which is a smooth function fitted to the multiply-discontinuous function $F(x, y)$. Figure 8 shows a contour plot of the surface $\hat{F}(x, y)$. It shows, for instance, that there are fewer than 20 seconds in the data base during which both the horn and dish notch depths simultaneously exceed 10 dB. There are fewer than 5 seconds

for which the notch depth on one antenna equals or exceeds 15 dB, while that on the other is 10 dB or greater.

Figure 8 was derived by first determining the values of the function $F(x, y)$ on a square grid of points, x_i, y_j, where

$$x_i = \begin{cases} 0 & i = 1 \\ i - 0.5 & i > 1 \end{cases}$$
$$y_j = \begin{cases} 0 & j = 1 \\ j - 0.5 & j > 1. \end{cases} \tag{25}$$

Since $F(x, y)$ falls off approximately exponentially with increasing values of x and y, we approximate it with $\hat{F}(x, y)$, where

$$\hat{F}(x, y) = \exp\left(- \sum_{m+n \le N} a_{mn} x^m y^n\right). \tag{26}$$

The coefficients a_{mn} in (26) were determined by minimizing the mean square error between $\ln \hat{F}(x, y)$ and $\ln F(x, y)$ over all x_i, y_j, less than 24 dB, for which there were five or more seconds in the data base, $F(x_i, y_j) \ge 5$. [The 5-second limit was chosen to avoid the region of the x, y plane where data is becoming sparse, causing the sample function, $F(x, y)$, to have increasingly extensive flat areas.] Figure 8 shows the equal value contours of $\hat{F}(x, y)$ as defined by (26) with $N = 6$, for which 28 parameters, a_{mn}, were determined.

The function $\hat{F}(x, y)$ with $N = 6$ provides an excellent representation of the sample function, $F(x, y)$; the rms error between $\ln \hat{F}(x, y)$ and $\ln F(x, y)$ is approximately 0.092, which corresponds to an rms error of 9.2 percent over the fitting region. While one can reduce the fitting error by increasing the dimension, N, of $\hat{F}(x, y)$, the reduction is not great. The minimum error, 6.7 percent, is obtained with $N = 9$ (55 coefficients, a_{mn}). Furthermore, the fitted functions, the $\hat{F}(x, y)$'s, lose the appearance of distribution functions for N greater than 6. Note that the distribution function, $F(x, y)$, must satisfy the inequality

$$F(x, y) \ge F(x', y') \quad \text{for} \quad x' \ge x, \, y' \ge y. \tag{27}$$

It may be seen that $\hat{F}(x, y)$ for $N = 6$, as shown in Fig. 8, violates this inequality for B_D near 1 dB and B_H greater than 12 dB.

An extensive study was undertaken to find a distribution function that would fit $F(x, y)$. While a function with a polynomial exponent such as $\hat{F}(x, y)$ can be fitted by solving a system of $(N + 1)(N + 2)/2$ linear equations, the more general distribution functions were fitted using a modified gradient search routine.[21] For practical reasons the class of functions was limited to those having no more than eight parameters. Of those tried, the best was of the form

$$F_M(x, y) = z_0(e^{-z_1 x^2} + z_3 e^{-z_2 x})(e^{-z_4 y^2} + z_6 e^{-z_5 y}). \tag{28}$$

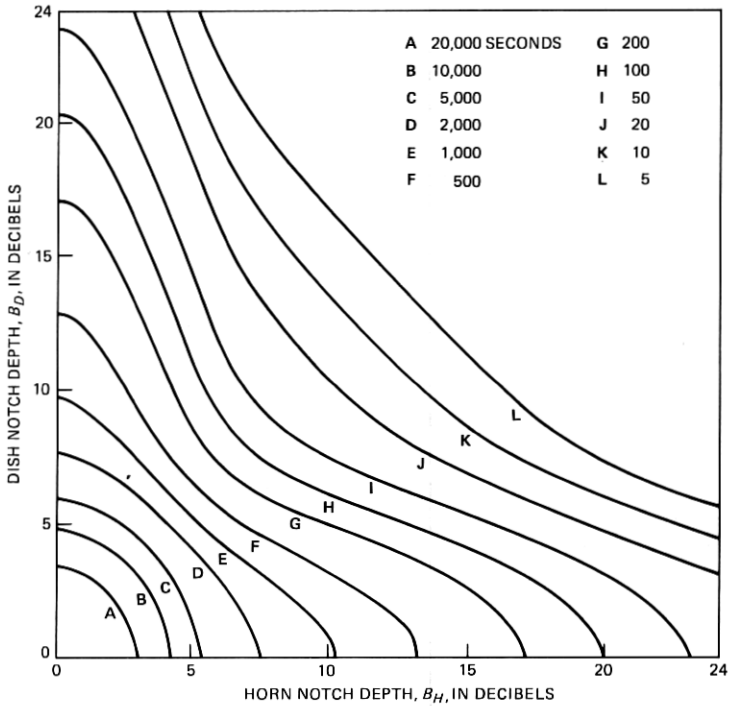

Fig. 9—Contour plot of $F_M(B_H, B_D)$, model cumulative joint distribution function of horn and dish relative notch depths.

For the parameter values corresponding to those in (12) and (13), the rms fitting error was 18.7 percent. The contour plot of this function, shown in Fig. 9, is seen to match the smoothed function of Fig. 8 quite closely. To show how well $F_M(x, y)$ matches the original sample distribution, we plot the distribution of horn notch depth conditioned on dish notch depth in Fig. 10, along with the values of the sample distribution, $F(x_i, y_j)$, being matched. A similar plot of the distribution of dish notch depth conditioned on horn notch depth is shown in Fig. 11.

Comparing Figs. 8 and 9, we see that the model function, $F_M(x, y)$, has most of the properties of the function $\hat{F}(x, y)$. From Figs. 10 and 11, one obtains an appreciation of the irregularities in the trends in the distribution of the data points; these irregularities contribute substantially to the fitting error. While one could argue that the modeling is acceptable on the basis of Figs. 8 to 11, there are more compelling reasons for accepting this distribution function as representing the data distribution, as we shall outline in the following paragraphs.

If the function used to represent the data distribution, $F(x, y)$, can be factored as a product of a function of x and a function of y, the

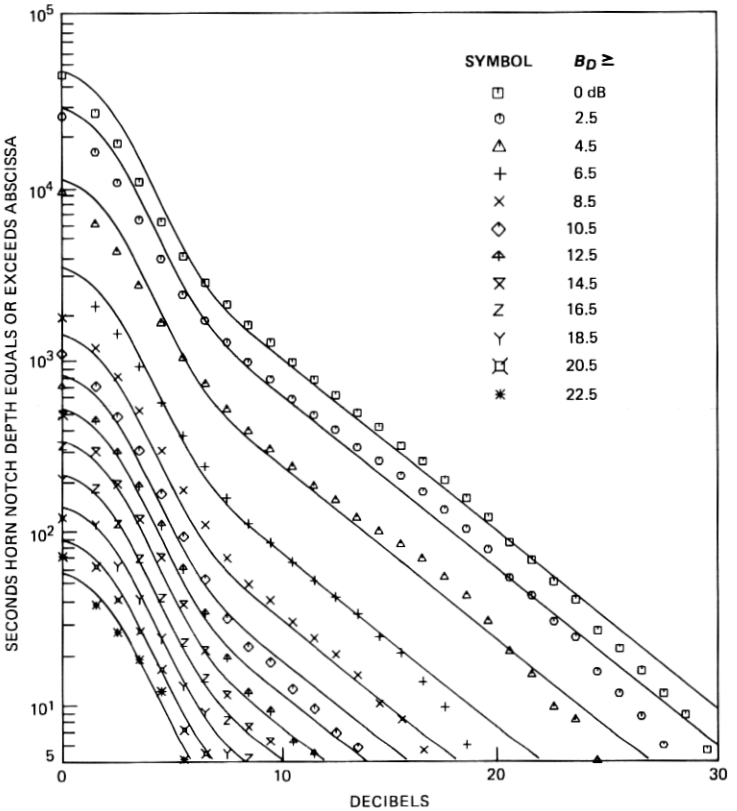

Fig. 10—Distribution of relative notch depth for the horn, conditioned on that for the dish.

resulting probability model will be one in which B_H and B_D are statistically independent. We will first show that the modeling function, $F_M(x, y)$, provides close to the minimum achievable error under the factorability assumption. Subsequently, we shall show that there is no reasonable alternative.

If the sample distribution were factorable, we could represent it exactly by

$$F_F(x, y) = c_0 \left[\exp\left(- \sum_{m=1}^{N} a_m x^m \right) \right] \left[\exp\left(- \sum_{n=1}^{N} b_n y^n \right) \right], \qquad (29)$$

since we are only representing the sample distribution at a finite number of points. Fitting a function of the form (29) to $F(x, y)$, as described previously, we find that the minimum rms error is 17.4 percent for $N = 7$, which corresponds to 15 terms. For larger dimensionality the error increases, presumably, because of loss of precision

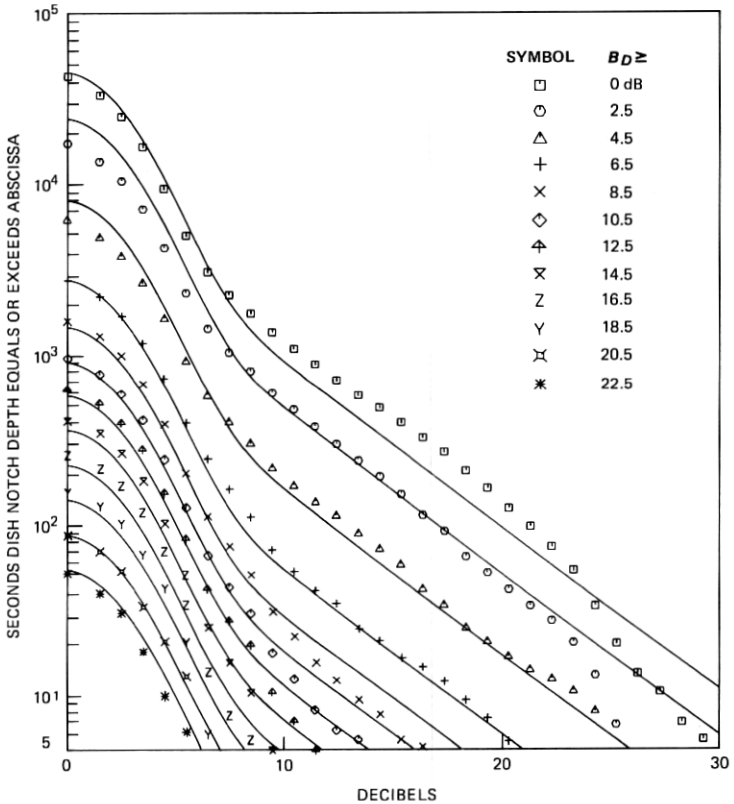

Fig. 11—Distribution of relative notch depth for the dish, conditioned on that for the horn.

in the double precision solution to the set of linear equations for the coefficients. The model solution achieves an rms error of 18.7 percent with fewer than half the number of coefficients.

As a check of the ruggedness of the model solution, we varied the region over which the model function was fitted. If the upper limit of x and y is reduced from 24 to 22 dB, the parameters change by less than one percent. If the region where both x and y are less than 5 dB is removed, the change is even smaller. We conclude that $F_M(x, y)$ provides an accurate and stable approximation to $F(x, y)$.

There is no way of testing whether B_H and B_D are statistically independent. One check, which we can apply, is to estimate their correlation coefficient. By examining the data base, we find that the coefficient of correlation between B_H and B_D is 0.0306. While there are standard tests for the significance of correlation coefficients,[22] they pertain to the case of independent sets of samples, whereas the time

series samples of the fading parameters we are working with are correlated.[23] In the appendix, we show that the effective number of independent time samples of B_H and B_D in the data base is approximately 1516, and that one would expect a correlation of this magnitude (0.0306) or greater about 27 percent of the time for this sample size.

Various subpopulations of the B-parameters were also examined for correlations. For instance, consider the set of B_H and B_D observations for which both were equal to or greater than 6 dB. The correlation coefficient is -0.118 for this subpopulation. It is shown in the appendix that a correlation coefficient of this magnitude or greater would be expected to occur 53 percent of the time.

Thus, we have based our choice of the model function $F_M(x, y)$ on the following grounds: (*i*) the model function (Fig. 9) captures the essential morphology of the sample distribution (Fig. 8); and (*ii*) no candidate distribution function providing correlation between B_H and B_D and employing a similar number of parameters represents the distribution function as well. While the rms error between the model distribution and the sample distribution is considerably larger than is that between the best functional representation, $\hat{F}(x, y)$, and the sample distribution, this is to be expected because $\hat{F}(x, y)$ has many more degrees of freedom and is not constrained to be a distribution function. In other words, $\hat{F}(x, y)$ represents the data within the region of interest by following all minor irregularities; immediately outside this region, this function exhibits large amplitude oscillations. By examining the correlation of B_H and B_D for various subpopulations we have established that there are correlations within these subpopulations. These correlations correspond to variations in the sample distribution surface that a factorable function, such as the model function, is incapable of matching, but which have been shown to be without significance. We conclude that there is no basis for choosing a more complicated function than (28) for representing the sample joint distribution.

4.3 Fade-level statistics

For the nondiversity fading model, the fade level or A-distribution was Gaussian with a mean dependent on the relative notch depth. A generalization of this, a two-dimensional Gaussian probability density function, describing the joint probability of A_H and A_D conditioned on B_H and B_D would be given by (14), with g_H, g_D, σ_H, σ_D, and ρ being functions of B_H and B_D. To obtain, for the diversity model, a probability density function that will easily reduce to that of the nondiversity model, we assume that g_H depends only on B_H, g_D depends only on B_D, and that σ_H, σ_D, and ρ are independent of both B_H and B_D.

As the first step in verifying this hypothesis, we must determine the

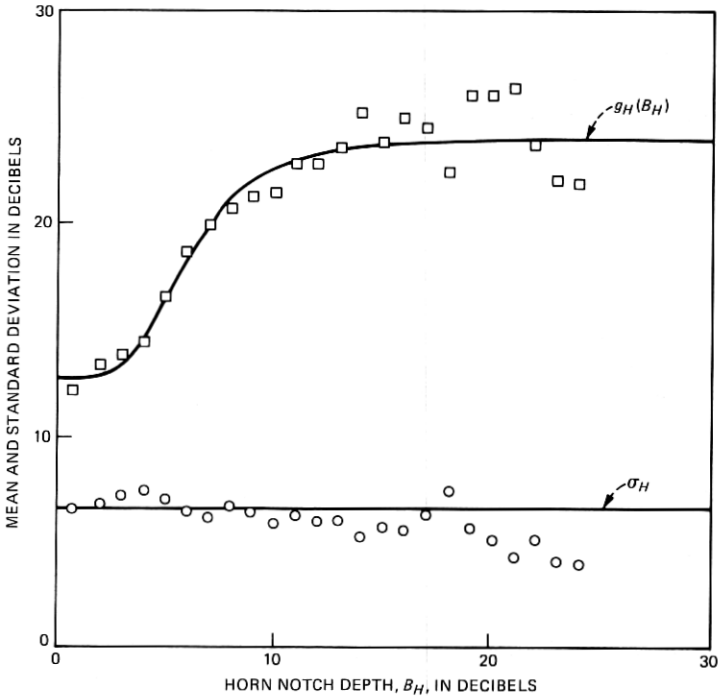

Fig. 12—Mean and standard deviation of A_H, fade-level parameter for the horn, as modeled and estimated for horn relative notch depth in 1-decibel intervals.

functional dependence of the means, g_H and g_D, on their respective variables, B_H and B_D. We do this by estimating the value of, say, g_H at a set of values of B_H, and fit a function to these sample means. The value of $g_H(x)$ is the average value of A_H for B_H equal to x. We estimate $g_H(x)$ by taking the expectation, or average value of A_H in the data base for all times that B_H is between $x - \delta$ and $x + \delta$. Specifically, we work with 1-dB intervals and estimate g_H by

$$\hat{g}_H\left(\frac{x_i + x_{i+1}}{2}\right) = E\{A_H : x_i \le B_H \le x_{i+1}\}, \tag{30}$$

where $E\{\cdot\}$ denotes expectation, and the x_i's are defined by (25).

The values of $\hat{g}_H(x)$ are indicated by squares in Fig. 12, which also shows the function $g_H(B_H)$ of (15), which we use as the conditional mean of A_H in the model. We use a meromorphic function, $g_H(B_H)$, to represent this conditional mean to ensure that it approaches a constant at large values of horn notch depth. Note that the accuracy of the estimates of $\hat{g}_H$ decrease at large values of the horn notch depth because the number of samples decreases. (The approximating function g_H was obtained from a weighted least-squares fit to the estimates,

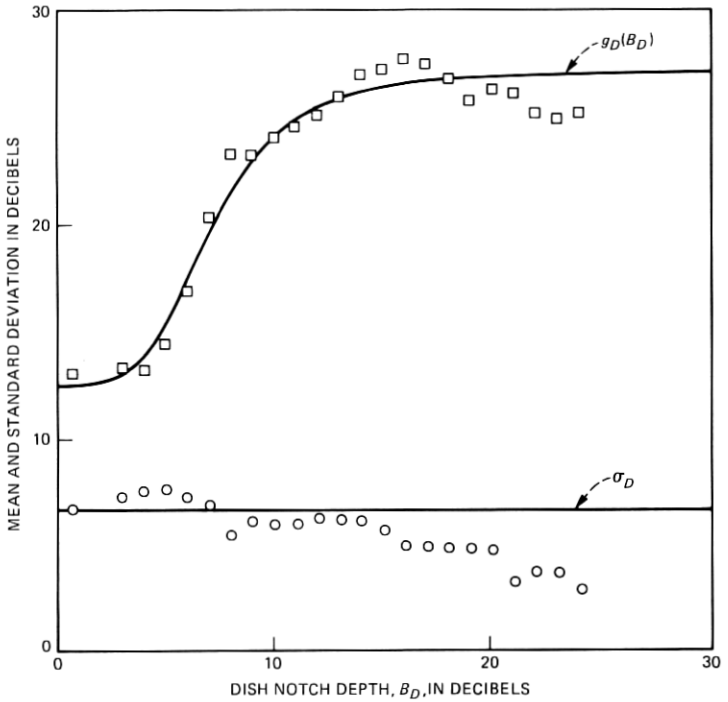

Fig. 13—Mean and standard deviation of A_D, fade-level parameter for the dish, as modeled and estimated for dish relative notch depth in 1-decibel intervals.

$\hat{g}_H$. The weighting was in proportion with the square root of the number of seconds of data in the notch depth interval.)

Figure 12 also shows the results of estimating the standard deviation of A_H conditioned on B_H in the same set of intervals. The straight line represents the (unconditional) standard deviation (6.8268) of $A_H - g_H(B_H)$ for the whole data base. Figure 13 shows the results of duplicating for the dish parameters the calculations leading to Fig. 12.

It is a simple matter to test the validity of the hypothesized model. If $A_H - g_H(B_H)$ and $A_D - g_D(B_D)$ are jointly Gaussian with zero means, correlation ρ, and respective standard deviations σ_H and σ_D, they may be linearly transformed into a pair of zero mean, unit-variance, independent, Gaussian random variables. We shall develop the transformation in two steps: a rotation of axes, followed by a scale change. Taking advantage of hindsight, we plot in Fig. 14 contours of the joint probability density for A_H and A_D of (14). The rotated axes x and y are defined by the transformation:

$$\begin{bmatrix} x \\ y \end{bmatrix} = \begin{bmatrix} \cos\theta & \sin\theta \\ -\sin\theta & \cos\theta \end{bmatrix} \begin{bmatrix} A_H - g_H(B_H) \\ A_D - g_D(B_D) \end{bmatrix}. \tag{31}$$

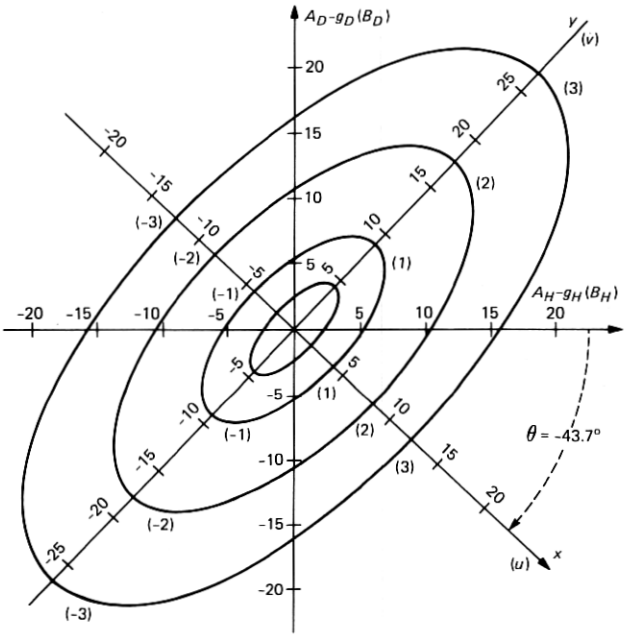

Fig. 14—Equal value contours of the joint conditional probability density function for fade-level parameters, A_H and A_D, showing variable transformations.

The chosen angle, θ (= −43.7 degrees), satisfies the relation

$$\tan 2\theta = \frac{2\rho\sigma_H\sigma_D}{\sigma_H^2 - \sigma_D^2}, \tag{32}$$

which ensures that x and y are uncorrelated. Their variances are given by

$$\sigma_x^2 = \sigma_H^2\cos^2\theta + \sigma_D^2\sin^2\theta + 2\rho\sigma_H\sigma_D\sin\theta\cos\theta \tag{33}$$

and

$$\sigma_y^2 = \sigma_H^2\sin^2\theta + \sigma_D^2\cos^2\theta - 2\rho\sigma_H\sigma_D\sin\theta\cos\theta, \tag{34}$$

respectively. From the variances and correlation in (17) and the value of θ given above, we calculate the values of σ_x and σ_y as 4.097 and 8.900, respectively. Note that the major axes of the ellipses of concentration shown in Fig. 14 lie along the y-axis, and the minor axes along the x-axis. By rescaling the x- and y-axes we obtain the desired zero mean, unit variance, independent variables, u and v, as

$$\begin{bmatrix} u \\ v \end{bmatrix} = \begin{bmatrix} 1/\sigma_x & 0 \\ 0 & 1/\sigma_y \end{bmatrix} \begin{bmatrix} x \\ y \end{bmatrix} \tag{35}$$

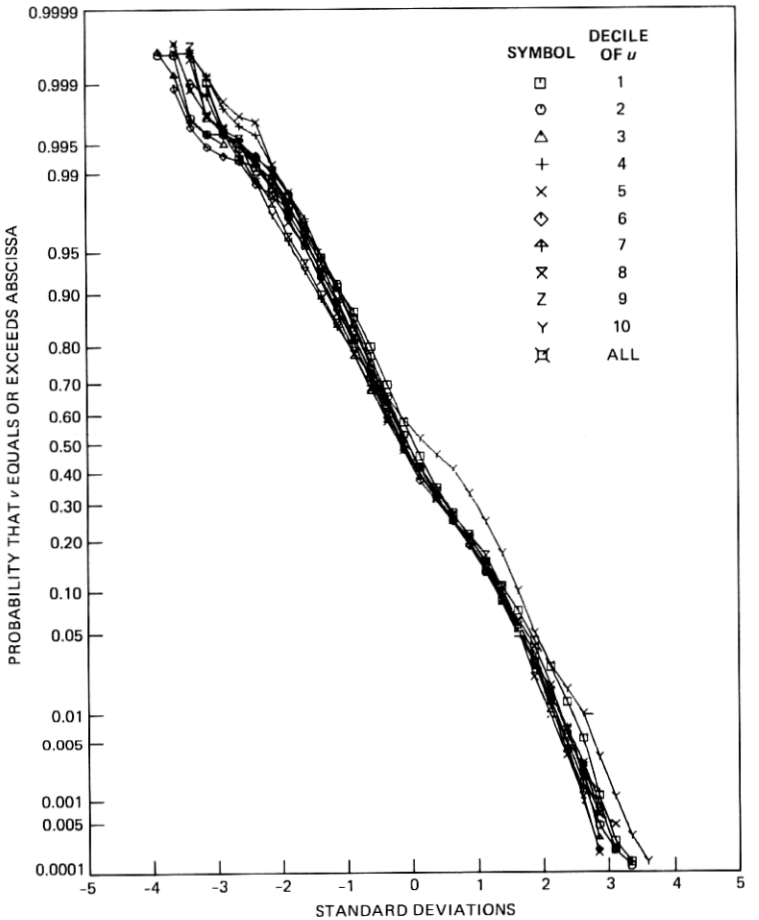

Fig. 15—Distribution of canonic sum parameter, v, conditioned on deciles of canonic difference parameter, u.

One may generate the sample distribution of u and v from the data base by calculating their values at each scan using eqs. (15) to (17) and (31) to (35). The conditional cumulative distribution functions of these two variables are shown in Figs. 15 and 16. Each plotted curve represents the cumulative distribution function of all values of one of the variables conditioned on the other variable being in a given decile of a Gaussian distribution; e.g., the first decile of u contains all u values that are less than -1.28155. Figure 15 shows the distributions of u conditioned on v; Fig. 16 shows v conditioned on u. Both families of distributions are closely grouped and approximately Gaussian within the range of -3 to $+3$ standard deviations. This is remarkably good agreement for a sample of this size.

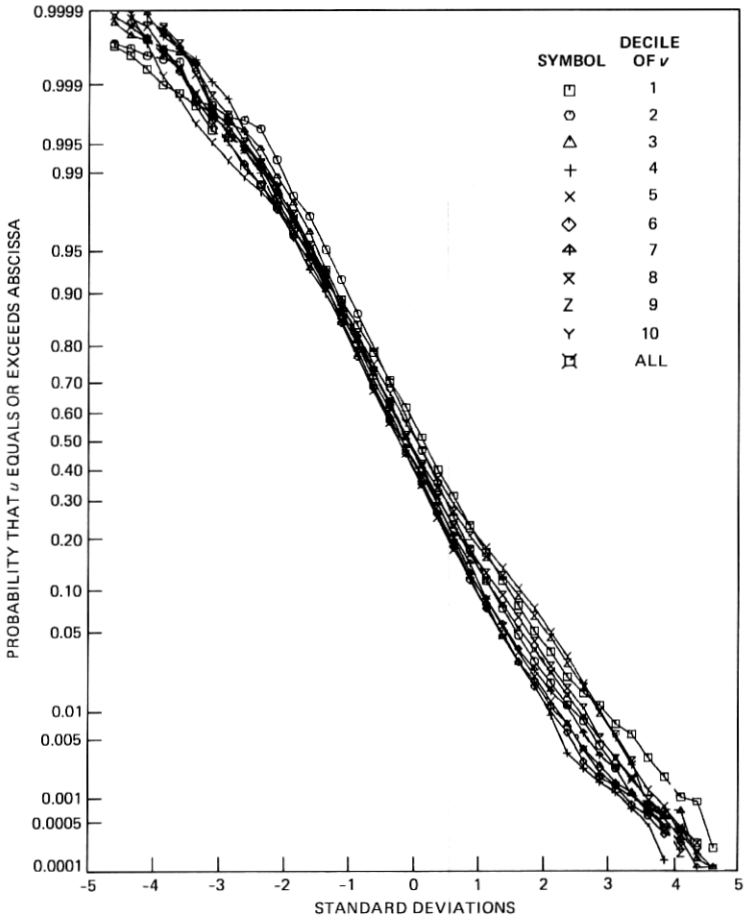

Fig. 16—Distribution of canonic difference parameter, u, conditioned on deciles of canonic sum parameter, v.

Figures 15 and 16 provide good confirmation of the assumption that A_H and A_D are jointly Gaussian variables. The only assumptions that were studied further were those relating to the functional form of g_H and g_D. The procedures outlined above were carried through under the assumption that g_H and g_D were both functions of both B_H and B_D. The resultant u and v conditional distribution functions were not noticeably different from Figs. 15 and 16. The only notable difference was that the value of σ_H was reduced from 6.8268 to 6.6815, that of σ_D from 7.0272 to 6.954, and the correlation coefficient increased from 0.650 to 0.681. This trivial difference in the coefficients would be achieved at considerable cost in complexity because the probability density function, (14), would become extremely difficult to use. The

effect of this generalized assumption is not pronounced on the functions g_H and g_D. For instance, the fractional variation of $g_H(B_H, B_D)$, as B_D varied its values along any line of constant B_H, was on the order of 10 percent. Hence, the development of a more complicated distribution cannot be justified.

4.4 Notch frequency statistics

As a first look for dependency between the horn and dish notch frequency parameters, the correlation coefficient between these two variables, ϕ_H and ϕ_D, was determined from the data base to be −0.0281. Using the techniques described in the appendix, one would expect a correlation magnitude larger than this value to occur 7.3 percent of the time in a data base of this size if ϕ_H and ϕ_D were statistically independent. While this correlation is small, it is large enough to be considered "almost significant" and to warrant a more detailed study.

The simplest way to look for the existence of any interdependency between the horn and dish notch frequencies is to plot distributions of one conditioned on the other. For instance, one chooses all those time intervals when the value of ϕ_D was between −85 and −65 degrees (or f_{0D} was between 37.4 and 28.6 MHz below the center frequency of the channel). One then plots the fraction of this time interval (2615 seconds) that the horn notch frequency exceeded a given value. The resulting conditional distribution is labeled by octagons on the composite plot of Fig. 17. The other distributions in Fig. 17 were obtained by conditioning the notch frequency on other intervals of dish notch frequency, as indicated. For reference, the span of the channel measurements is from −27.5 to +27.5 degrees (±12.1 MHz).

Since the overall spread of this family of distributions is small (less than 10 percent), over the range of ϕ_H, we represent the entire family by a single distribution, (18), shown dashed. Thus, we describe the distribution as uniform at two levels with values of $|\phi_H|$ less than 90 degrees being five times as likely as values greater than 90 degrees.

Figure 18 shows a set of distributions of the dish notch frequency conditioned on the horn notch frequency. This family of distributions is very tightly clustered, implying that the horn notch position had no influence on the distribution of dish notch position. The family of dish notch distributions does not fit the two-level uniform approximation, shown dashed in Fig. 18, as well as does the horn data. The relatively large deviation (about 15 percent near −30 degrees) between the data and the modeled distributions results from an asymmetry in the data, where, on a physical basis, none should be found. For atmospheric multipath, one expects transmission notches to be equally likely at any frequency in the neighborhood; hence, the notch frequency probability density functions should be symmetric and the cumulative distribution

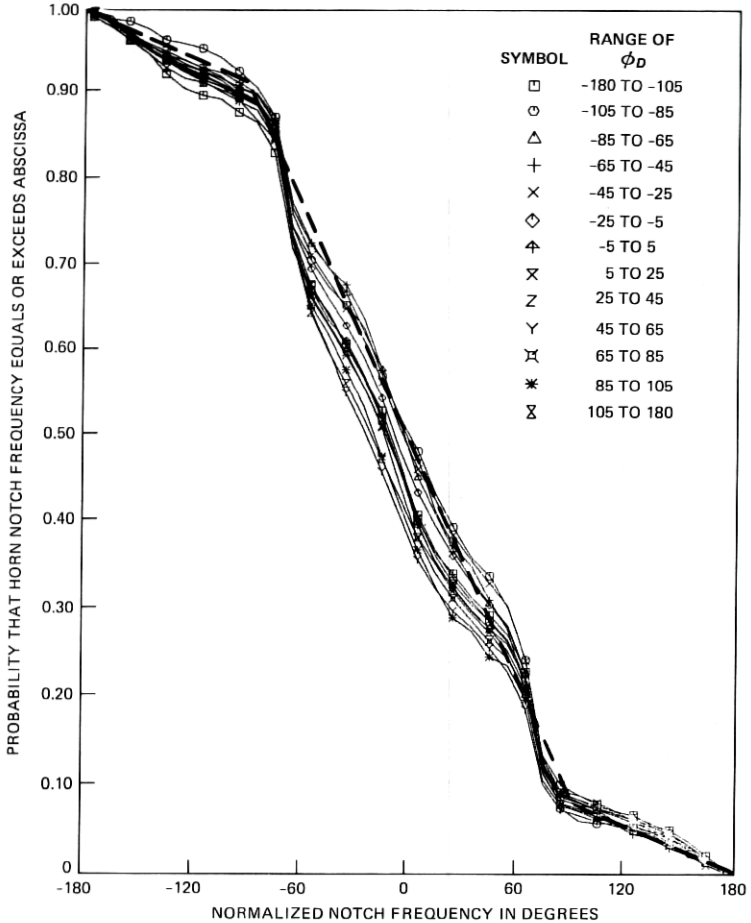

Fig. 17—Distribution of horn notch frequency conditioned on dish notch frequencies in specified intervals.

functions shown should be antisymmetric about the (0 degree, 50 percent) point.

In the central 60-degree region of the horn notch frequency distribution, the distributions conditioned on positive dish notch frequencies cluster separately from those conditioned on negative frequencies. This is an integrated effect, in that it is not apparent in the conditional probability density functions (not shown). There may be some relation between this spread in the horn notch frequency distribution, the spreading of the time-faded statistics for the dish (Fig. 4), and the symmetry properties of the observed dish notch frequency distribution (noted in Fig. 18). However, these differences are small and no attempt

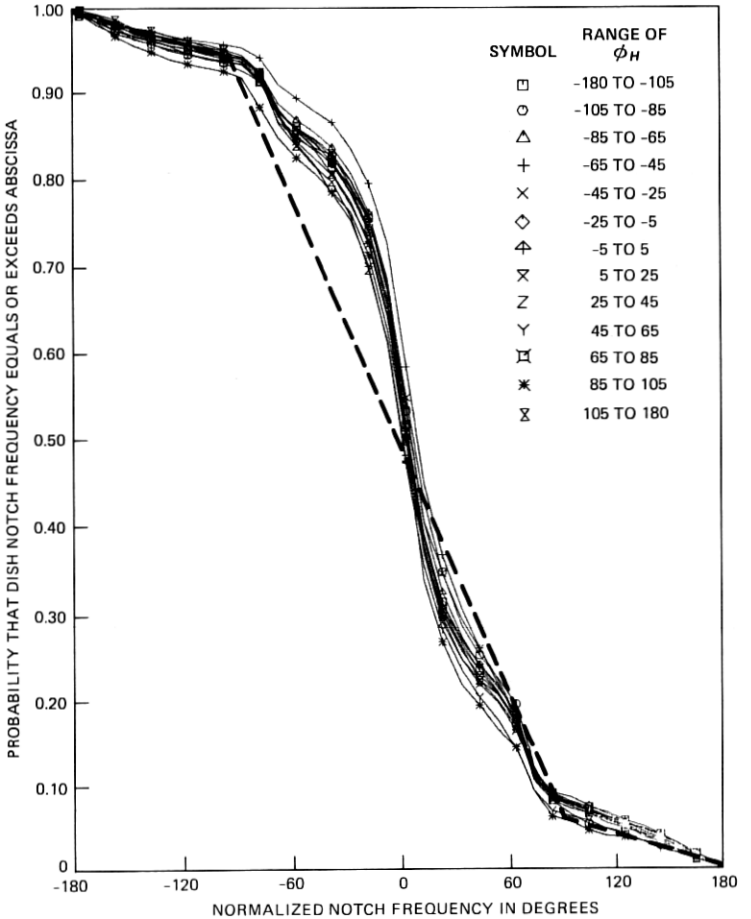

Fig. 18—Distribution of dish notch frequency conditioned on horn notch frequencies in specified intervals.

was made to isolate the events giving rise to these effects or to incorporate them into the model.

V. CONCLUDING REMARKS

We have provided in Section II a statistical model of multipath fading as observed in a diversity configuration over an extended period of time. Supporting evidence of the accuracy of the statistical model was presented in Section IV, along with a description of the methodologies employed. The transmission path to each antenna was represented by a function synthesizing a simplified three-path fade. While one could statistically represent the joint occurrence of the parameters

of these two functions in the observed data base with greater precision using a more complex model, all attempts to establish the significance of higher order extrapolations of the proposed statistical model have been negative. There would seem to be little virtue in representing, with a particular statistical model, features that would not be found in a fading data base corresponding to a different observation period.

For the proposed model, the only correlation in the fading of the two antennas is in the level of fade. This simplicity of dependence is a direct result of the form of the function used to represent fading on the two antennas. More, or different, interdependencies might become apparent or significant with other fade representations. The limited dependence is a virtue of the model since it places all of the impact of diversity antenna separation in a single parameter, for separations in the range of practical interest. However, for sufficiently small separation one would ultimately expect to see correlations in the shapes of the fades observed on the two antennas.

The proposed model was only checked against the data; however, it reduces to the form of the nondiversity model, which has been extensively verified. A model representing fading on the horn is obtained by integrating the model statistics over the dish parameters, and vice versa. Some of the parameters of the horn and dish models derived from the diversity model are different from those that have been derived previously, but the differences are not great, on the order of 10 percent, at most. As a consequence, one would not be surprised by 20 to 30 percent differences between expectations calculated with this model and corresponding expectations calculated with the nondiversity model. This merely reflects the month-to-month and year-to-year variability in the nature and severity of multipath fading.

ACKNOWLEDGMENT

This study would not have been possible without the contributions of many individuals. The radio equipment was installed, aligned, and maintained by R. A. Hohmann, C. W. Lundgren, and L. J. Morris, with instrumentation designed by G. A. Zimmerman. The data base was assembled and calibrated by D. W. Rowland under the guidance of M. V. Pursley, who also generated Figs. 3 to 5. C. H. Menzel provided much useful advice for the efficient utilization of computer resources and maintained the viability of these resources frequently at odd hours in the face of rolling waves of hardware/software catastrophies. The insights into the data would not have been possible without the plotting packages developed by A. K. Ranade. For many stimulating discussions of this work and comments on this manuscript, I would like to thank W. T. Barnett, S. H. Lin, W. W. Toy, T. S. Giuffrida, V.

K. Prabhu, and other members of the Transmission Systems Characterization Department.

REFERENCES

1. W. T. Barnett, "Multipath Fading Effects on Digital Radio," IEEE Trans. Commun., *COM-27*, No. 12 (December 1979), pp. 1842–48.
2. C. W. Anderson, S. G. Barber, and R. N. Patel, "The Effect of Selective Fading on Digital Radio," IEEE Trans. Commun., *COM-27*, No. 12 (December 1979), pp. 1870–76.
3. T. S. Giuffrida, "Measurements of the Effects of Propagation on Digital Radio Systems Equipped with Space Diversity and Adaptive Equalization," in Conf. Rec., 1979 Int. Conf. on Commun., Vol. *3*, pp. 48.1.1–6.
4. W. W. Toy, "The Effects of Multipath Fading on 16 QAM Digital Radio," in Conf. Rec., 1980 Int. Conf. Commun., Vol. *3*, pp. 52.1.1–5.
5. T. S. Giuffrida, "The Effects of Multipath Fading Upon Adjacent Channel Operation of an 8 PSK 6 GHz Digital Radio," in Conf. Rec., 1980 Int. Conf. on Commun., Vol. 2, pp. 34.1.1–5.
6. W. D. Rummler, "More on the Multipath Fading Channel Model," IEEE Trans. Commun., *COM-29*, No. 3 (March 1981), pp. 346–52.
7. W. D. Rummler, "A New Selective Fading Model: Application to Propagation Data," B.S.T.J., *58*, No. 5 (May–June 1979), pp. 1037–72.
8. C. W. Lundgren and W. D. Rummler, "Digital Radio Outage Due to Selective Fading—Observation vs. Prediction From Laboratory Simulation," B.S.T.J., *58*, No. 5 (May–June 1979), pp. 1073–1100.
9. A. J. Giger and W. T. Barnett, "Effects of Multipath Propagation on Digital Radio," IEEE Trans. Commun., *COM-29*, No. 9, (September 1981), pp. 1345–52.
10. T. S. Giuffrida and W. W. Toy, "16 QAM and Adjacent Channel Interference," in Conf. Rec., 1981 Int. Conf. on Commun., Vol. *1*, pp. 13.1.1–5.
11. L. J. Greenstein and B. A. Czekaj, "A Polynomial Model for Multipath Fading Channel Responses," B.S.T.J., *59*, No. 7 (September 1980), pp. 1197–1225.
12. W. C. Jakes, Jr., "An Approximate Method to Estimate an Upper Bound on the Effect of Multipath Delay Distortion on Digital Transmission," IEEE Trans. Commun., *COM-27*, No. 1 (January 1979), pp. 76–81.
13. L. J. Greenstein and V. K. Prabhu, "Analysis of Multipath Outage with Applications to 90 Mbit/s PSK Systems at 6 and 11 GHz," IEEE Trans. Commun., *COM-27*, No. 1 (January 1979), pp. 68–75.
14. J. Sandberg, "Extraction of Multipath Parameters from Swept Measurements on a Line-of-Sight Path," IEEE Trans. Antennas and Propagation, *AP-28*, No. 6 (November 1980), pp. 743–50.
15. L. Martin, "Etude de la Selectivite des Evanouissements dus aux Trajets Multiples," Ann. Telecommunic., *35*, No. 11–12 (November–December 1980), pp. 482–7.
16. F. Andreucci, F. Fedi, and P. G. Marchetti, "Analytical Method to Evaluate the Effect of Multipath Fading on Long-Haul High-Capacity Digital Radio Relay Systems," Ann. Telecommunic., *35*, No. 11–12 (November–December 1980), pp. 488–93.
17. E Damosso and S. DePadova, "A Statistical Model for the Evaluation of the Impairments Due to Multipath Fades on Digital Radio Links," in Conf. Rec., 1981 Int. Conf. on Commun., Vol. *4*, pp. 68.7.1–5.
18. W. T. Barnett, "Multipath Propagation at 4, 6, and 11 GHz," B.S.T.J., *51*, (February 1972), pp. 321–61.
19. A. Vigants, "Space-Diversity Engineering," B.S.T.J., *54*, No. 1 (January 1975), pp. 103–41.
20. W. D. Rummler, "Time- and Frequency-Domain Representation of Multipath Fading on Line-of-Sight Microwave Paths," B.S.T.J., *59*, No. 5 (May–June 1980), pp. 763–796.
21. P. R. Bevington, *Data Reduction and Error Analysis for the Physical Sciences*, New York: McGraw-Hill Book Company, 1969.
22. H. Cramer, *Mathematical Methods of Statistics*, Princeton, N.J.: Princeton University Press, 1946.
23. W. D. Rummler, "Advances in Multipath Channel Modeling," in Conf. Rec., 1980 Int. Conf. on Commun., Vol. *3*, pp. 52.3.1–5.

APPENDIX

Correlation and Significance

The purpose of this appendix is to develop the methods of testing for the significance of the correlation between two random variables when the sample values of each variable are taken from a time series with known autocorrelation. Consider two stationary, independent, zero mean, unit variance random processes, $x(t)$ and $y(t)$. Assume that we have samples of each at a large number, N, of time instants, where the ith time instant is taken as

$$t_i = i\Delta t \qquad i = 1, 2, 3, \cdots, N. \tag{36}$$

We are interested in the correlation coefficient of x and y as determined from the set of samples $x_i = x(t_i)$ and $y_i = y(t_i)$, where

$$\rho = \frac{1}{N} \sum_{i=1}^{N} x_i y_i. \tag{37}$$

Because $x(t)$ and $y(t)$ are independent processes by assumption, the expected value of ρ is zero:

$$\bar{\rho} = \frac{1}{N} \sum_{i=1}^{N} \overline{x_i y_i} = 0, \tag{38}$$

where the overbar implies an ensemble average.

We wish to determine the variance of the estimate (37). We write the expected value of this sample variance as

$$\sigma_\rho^2 = \overline{\rho^2} = \frac{1}{N^2} \sum_{i=1}^{N} \sum_{j=1}^{N} \overline{x_i y_i x_j y_j}. \tag{39}$$

Under the hypothesis that $x(t)$ and $y(t)$ are independent processes, we may rewrite (39) as

$$\sigma_\rho^2 = \frac{1}{N^2} \sum_{i=1}^{N} \sum_{j=1}^{N} \overline{x_i x_j}\, \overline{y_i y_j} = \frac{1}{N^2} \sum_{i=1}^{N} \sum_{j=1}^{N} \rho_x(i-j)\rho_y(i-j), \tag{40}$$

where

$$\rho_x(i) = \overline{x_k x_{k+i}} \tag{41}$$

and

$$\rho_y(i) = \overline{y_k y_{k+i}} \tag{42}$$

are the autocorrelation functions of $x(t)$ and $y(t)$, respectively, at time difference $i\Delta t$. We may rewrite (40) as

$$\sigma_\rho^2 = \frac{1}{N^2} \left[N + 2 \sum_{k=1}^{N} (N-k)\rho_x(k)\rho_y(k) \right]. \tag{43}$$

If the time samples of $x(t)$ and $y(t)$ were independent, the autocor-

relation functions would be unity for $k = 0$ and zero elsewhere, that is,

$$\sigma_\rho^2 = \frac{1}{N} \quad \text{if} \quad \rho_x(i) = \rho_y(i) = 0 \quad \text{for} \quad i \neq 0. \tag{44}$$

Let us define an effective sample size, N_{eff}, such that, for a given sample size, N, and given autocorrelation functions, $\rho_x(i)$ and $\rho_y(i)$,

$$\sigma_\rho = \frac{1}{\sqrt{N_{eff}}}. \tag{45}$$

Then,

$$\frac{N}{N_{eff}} = 1 + 2 \sum_{k=1}^{N} \left(\frac{N-k}{N} \right) \rho_x(k)\rho_y(k). \tag{46}$$

Our object is to use (45) and (46) for the diversity data base. As noted in Section III, the data base is not uniformly sampled. Furthermore, multipath fading is not a stationary random process. One may, however, define a lagged autocorrelation function for the samples of such a process[23] at delay τ as

$$\rho_x(\tau) = \frac{\left(\frac{1}{M}\sum x_m x_{m+\tau}\right) - \left(\frac{1}{M}\sum x_m\right)\left(\frac{1}{M}\sum x_{m+\tau}\right)}{\left[\left(\frac{1}{M}\sum x_m^2\right) - \left(\frac{1}{M}\sum x_m\right)^2\right]^{1/2}\left[\left(\frac{1}{M}\sum x_{m+\tau}^2\right) - \left(\frac{1}{M}\sum x_{m+\tau}\right)^2\right]^{1/2}}, \tag{47}$$

where the sample denoted $x_{m+\tau}$ is τ seconds delayed from the sample x_m, and the sums are taken over all $M = M(\tau)$ pairs of samples in the data base with a delay difference of τ.

Figure 19 shows plots of (47) for: (a) the relative notch depth of the horn, and (b) the relative notch depth of the dish. Figure 20 shows $M(\tau)$, the sample size for the data base, as a function of the delay, τ, for delays of integer numbers of seconds. Using these two figures as examples, we can approximate the quantity N/N_{eff}. We describe the autocorrelation functions by

$$\rho_x(\tau) = \alpha_x e^{-\tau/\tau_x} = \alpha_x \beta_x^\tau \tag{48}$$

and

$$\rho_y(\tau) = \alpha_y e^{-\tau/\tau_y} = \alpha_y \beta_y^\tau. \tag{49}$$

The samples in the data base are taken nonuniformly in a set of disjoint intervals. With 85,410 samples in 44,386 seconds we have an average sample spacing of 0.5 second. Hence, we approximate the uniform-sampling window function of (46), $(N - k)/N$, by taking an approximation to $M(\tau)/N$, as shown in Fig. 20 and given by

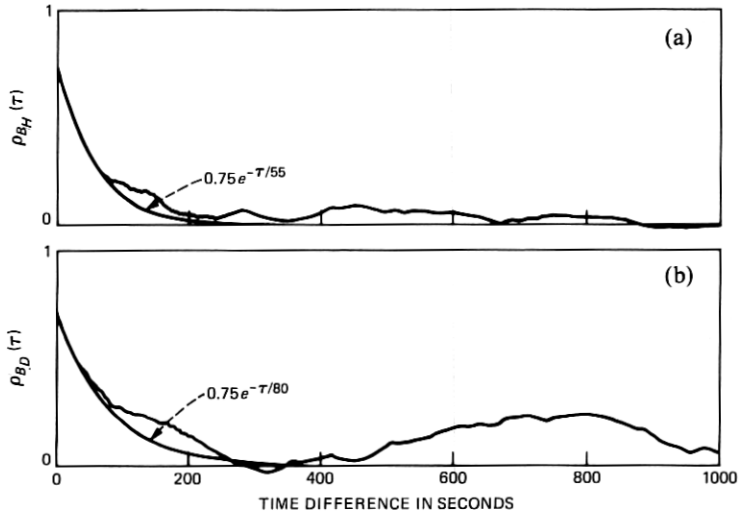

Fig. 19—Autocorrelation of lagged samples of relative notch depth for (a) horn and (b) dish.

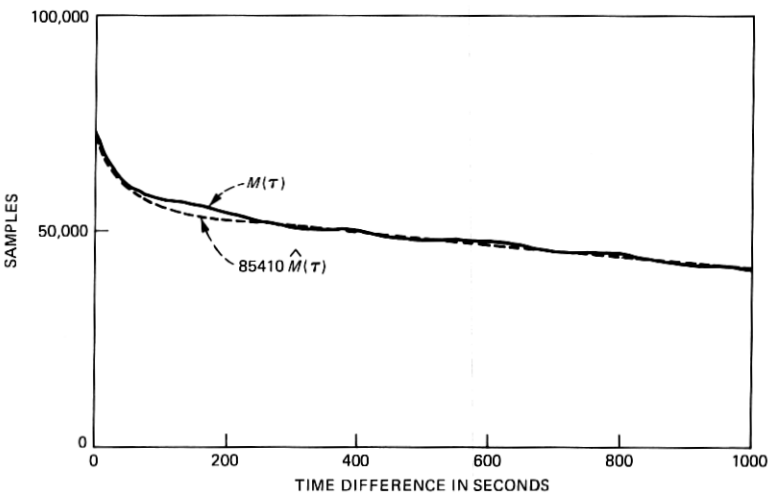

Fig. 20—Sample size for autocorrelation estimates in Fig. 19.

$$\hat{M}(\tau) = \frac{M(\tau)}{N} = \frac{3.5}{17}\, e^{-\tau/45} + \frac{11}{17}\left(1 - \frac{\tau}{4000}\right) \quad \tau \leq 4000. \tag{50}$$

Using (48) to (50) with $\tau = 0.5\ k$ corresponding to the 0.5 second average sampling interval, we rewrite (46) as

$$\frac{N}{N_{eff}} = 1 + 2 \sum_{k=1}^{N} \hat{M}(k/2)\alpha_x\alpha_y(\beta_x\beta_y)^{k/2} \tag{51}$$

or

$$\frac{N}{N_{eff}} = 1 + \frac{2\alpha_x\alpha_y}{17}\left\{\frac{3.5re^{-1/90}}{1-re^{-1/90}} + \frac{11r}{1-r}\left[1 - \frac{1}{8000(1-r)}\right]\right\}, \quad (52)$$

where

$$r = (\beta_x\beta_y)^{0.5}. \quad (53)$$

Consider the horn and dish relative notch depths, B_H and B_D, respectively. Letting $B_H = x$ and $B_D = y$,

$$\alpha_x = \alpha_y = 0.75$$
$$\beta_x = e^{-1/55}$$
$$\beta_y = e^{-1/80}$$
$$r = 0.98478. \quad (54)$$

Therefore, from (51) to (54),

$$\frac{N}{N_{eff}} \approx 56.3. \quad (55)$$

For the data base, the calculated value of the correlation coefficient of B_H and B_D was 0.0306 for the entire set of 85,410 samples. From (55), $N_{eff} = 1516$. Using this in (45), we find $\sigma_\rho = 0.0257$. Under the unfavorable assumption[22] that the distribution of ρ is normal, we would expect to find a value of $|\rho|$ this large ($1.19\sigma_\rho$) or greater to occur for less than 27 percent of the samples of this size.

Similarly, for the case of a subpopulation of 1608 samples of B_H and B_D, whose correlation coefficient was -0.118, we find from (55) that $N_{eff} = 28.5$, and from (45) that $\sigma_\rho = 0.187$. We would expect to find a value of $|\rho|$ this large ($0.63\sigma_\rho$) or greater to occur for less than 53 percent of the samples of this size. One concludes that in neither of these two cases does the correlation differ significantly from zero.